HAL
open science

Heat Dissipation Test With Fiber-Optic Distributed Temperature Sensing to Estimate Groundwater Flux

Laura del Val, Jesús Carrera, María Pool, Lurdes Martínez, Carlos Casanovas, Olivier Bour, Albert Folch

To cite this version:

Laura del Val, Jesús Carrera, María Pool, Lurdes Martínez, Carlos Casanovas, et al.. Heat Dissipation Test With Fiber-Optic Distributed Temperature Sensing to Estimate Groundwater Flux. Water Resources Research, 2021, 57 (3), pp.e2020WR027228. 10.1029/2020WR027228 . insu-03185511

HAL Id: insu-03185511

https://insu.hal.science/insu-03185511v1

Submitted on 30 Mar 2021

HAL is a multi-disciplinary open access archive for the deposit and dissemination of scientific research documents, whether they are published or not. The documents may come from teaching and research institutions in France or abroad, or from public or private research centers.

L'archive ouverte pluridisciplinaire **HAL**, est destinée au dépôt et à la diffusion de documents scientifiques de niveau recherche, publiés ou non, émanant des établissements d'enseignement et de recherche français ou étrangers, des laboratoires publics ou privés.

Check for updates

AGU ADVANCING EARTH AND SPACE SCIENCE

Water Resources Research

RESEARCH ARTICLE

10.1029/2020WR027228

Heat Dissipation Test With Fiber-Optic Distributed Temperature Sensing to Estimate Groundwater Flux

Laura del Val[1,2,3], Jesús Carrera[2,4], María Pool[2,4], Lurdes Martínez[1,2], Carlos Casanovas[2,4], Olivier Bour[5], and Albert Folch[1,2]

[1]Department of Geotechnical Engineering and Geosciences, Universitat Politecnica de Catalunya (UPC), Barcelona, Spain, [2]Associated Unit: Hydrogeology Group (UPC-CSIC), Barcelona, Spain, [3]Department of Earth and Ocean Dynamics, University of Barcelona (UB), Barcelona, Spain, [4]Institute of Environmental Assessment and Water Research (IDAEA), Consejo Superior de Investigaciones CIentificas (CSIC), Barcelona, Spain, [5]Géosciences Rennes, University of Rennes, CNRS, Rennes, France

Key Points:

- Groundwater flux is quantified by performing a heating test with a single fiber-optic cable installed outside de borehole casing
- A new analytical approach to estimate groundwater flux with a heat dissipation test employing fiber optics is proposed
- The method interprets tests performed with a single cable in a single borehole, saving the costs of drilling observation boreholes

Correspondence to:

L. del Val,
lauradelvalalonso@gmail.com

Citation:

del Val, L., Carrera, J., Pool, M., Martinez, L., Casanovas, C., Bour, O., & Folch, A. (2021). Heat dissipation test with fiber-optic distributed temperature sensing to estimate groundwater flux. *Water Resources Research*, *57*, e2020WR027228. https://doi.org/10.1029/2020WR027228

Received 28 JAN 2020
Accepted 2 FEB 2021

© 2021. American Geophysical Union. All Rights Reserved.

Abstract We measure groundwater flux and thermal parameters around a borehole performing a heat dissipation test by heating the armor of a single fiber-optic cable and interpreting the resulting heating curves with a new analytical method. The procedure is similar to thermal response tests, but benefitting from the high spatial and temporal resolution of distributed temperature sensing and lasting longer, so as to measure advective dissipation. Field installation relies on an innovative method in hydrogeology, which is based on the installation of the FO cable in the annular space of the well, close to the aquifer matrix. The proposed new analytical method, expands the traditional Moving Infinitesimal Line Source Model to account for the effects of the field set up and cable materials. In fact, we show that the resulting temperature build-up goes through four periods easy to identify using the log derivative of temperature (dT/d (ln(t))): Initial response, skin (cable insulation), conduction dominated and advection dominated. We test the proposed method in an unconsolidated shallow aquifer with controlled pumping. Results are of the same order of magnitude of independent estimates of groundwater velocity.

1. Introduction

Quantification of groundwater velocity is desirable for numerous hydrogeological problems, ranging from contaminant migration to submarine groundwater discharge quantification, and from geothermal systems optimization to leakage identification. Unfortunately, available methods for measuring natural groundwater velocity in aquifers present several drawbacks. The most reliable estimates of natural flux can be obtained through solute and/or heat tracing (Anderson, 2005; Bakker et al., 2015; Davis et al., 1985; des Tombe et al., 2019; Read et al., 2013; Reiter, 2001; Sellwood et al., 2015; Taniguchi, 1993). However, natural flow tracing is expensive (several observation wells are needed and tests may require a long duration), risky (the observation network may fail to capture the plume), often hard to interpret and, as a result, rarely repeated over time for characterizing time variability. A single well method would be more desirable than the methods that need separated heating lines, additional observation points or the injection of tracers (hot water), as this would significantly simplify its implementation in the field and save costs.

These conditions are partially met by heat and solute dilution methods, which relate the flow rate to the observed variations of a known initial tracer concentration or heat pulse placed within the well. These tests have been widely used, and therefore validated (Drost et al., 1968; Jamin et al., 2015; Pitrak et al., 2007, among others). Arguably, the most sophisticated of these are fluid logging methods (Tsang et al., 1990), which consist of replacing the borehole fluid and measuring how some fluid property (e.g., electrical conductivity) evolves over time along the borehole. Variations of the method can be used to measure and quantify zones of increased groundwater inflow, hydraulic fracture interconnectivity (Jamin et al., 2015) and to identify velocity within the borehole (Drost et al., 1968). These measurements are useful and can be used to derive aquifer properties, but they yield flow rates within the borehole, which are not completely representative of the flux in the porous matrix. The design of a method allowing the collection and interpretation of data closer to the porous matrix would be appreciated. This is the case of some new methods involving fiber optic distributed temperature sensing (FO-DTS) (Bakker et al., 2015; des Tombe et al., 2019)

The high spatial and temporal resolutions of FO-DTS techniques have opened the way for improved thermal tracing. This is especially true for active FO-DTS, which consists of heating the FO cable or the media around the monitoring cable, and monitoring the ensuing temperature increase (Freifeld et al., 2008). Active FO-DTS have been employed as a thermal response test (Freifeld et al., 2008), as a fluid logging technique (Banks et al., 2014) and for heat tracing (Bakker et al., 2015; Hausner et al., 2016). However, the best way to employ this technology is still under discussion due to the different issues raised during: (i) interpretation of results, (ii) correction of FO cable thermal effects, and (iii) installation of the cable.

With respect to the installation of FO in the borehole, several configurations have been proposed, while the best approach remains an open question, usually leading to case specific set-ups. For active FO-DTS, some authors installed separate heating and monitoring lines (Bakker et al., 2015; Banks et al., 2014; Hausner et al., 2016; Leaf et al., 2012; Liu et al., 2013; Selker & Selker, 2018). A few authors simplified the installation by using the same cable for heating and monitoring (Coleman et al., 2015; Perzlmaier et al., 2004; Read et al., 2014; Su et al., 2016). In parallel, the same studies proposed different approaches for the installation of the cable in the ground. Initial studies deployed the cable within the well (Coleman et al., 2015; Hausner et al., 2016; Klepikova et al., 2011; Liu et al., 2013), which is the most simple and nonpermanent field strategy. In these cases, groundwater flow within the well might be affected by natural convection. Coleman et al. (2015) and later Maldaner et al. (2018) used a lining filled with water to hinder convection. Likewise, Selker & Selker (2018) permanently filled the borehole in order to prevent any effect of free water movement. A different approach is proposed by Bakker et al. (2015) and des Tombe et al. (2019) by installing the cables with direct push equipment leaving the aquifer materials to collapse around the cable. Heating curves produced by this method are the most representative from aquifer conditions. However, this installation has two main limitations: A depth limit of around 60 m and impossibility for installation in certain geologic materials such as gravels. An alternative would be to install the cable permanently between the borehole casing and the aquifer materials. This has already been done for monitoring of CO_2 storage boreholes (Freifeld et al., 2008; Giese et al., 2009). However, in the application reported by Giese et al. (2009) the cable was covered by the casing cementation. Installation of the FO cable behind the borehole casing, in contact with the aquifer materials, is not customary in hydrogeology applications (Bense et al., 2016). Still, this way would allow the cable to be in direct contact with the aquifer material, which may be advantageous in applications aiming to quantify groundwater fluxes.

Beyond this discussion, the most important question of how to better measure natural aquifer flux employing fiber-optic cables and DTS technology remains open. Perzlmaier et al. (2004) proposed a semi-empirical solution to estimate dam leakage by combining the steady state solution of a cylindrical heat exchanger, with the estimation of empirical factors. Su et al. (2016) used a numerical approach to investigate the relationship between effective thermal conductivity and seepage velocity through an experimental sand tank. Selker & Selker (2018) proposed heating at spaced intervals to measure both radial heat dissipation and vertical fluxes. However, the methology used in the interpretation of the obtained heating curves can only estimate relative velocities. In summary, formal analytical methods for estimating absolute groundwater fluxes using a single heating and monitoring cable have not been established yet.

Additionally, the effect of the cable materials and surrounding installation in the heat transport and therefore, in the temperature curves measured by the FO cable, is overlooked in most of the applications found in the literature. Probably because most of them use separated heating and measuring lines, in which cases this effect is neglectable. But it becomes important when dealing with a single heating and measuring line. This effect is analog to the "skin effect" in well hydraulics (Feng & Zhan, 2016) or the "borehole thermal resistance" in geothermal thermal response tests (TRT) (Bandos et al., 2011; Raymond et al., 2011; Wagner et al., 2013). In TRTs thermal influence of the well structure is considered explicitly as a factor, named the "borehole thermal resistance" (m K W^{-1}), which corrects for the excess of temperature increase due to the temperature storage in the borehole materials. Likewise, in well hydraulics the skin effect may increase or decrease drawdown at the pumping well because permeability around the well casing may be larger or smaller, respectively, than the formation permeability, which causes uncertainty in the estimation of storativity (Sánchez-Vila et al., 1999). The same phenomena is described by Cardenas (2010) associated to the use of temperature measured in pipes to quantify vertical groundwater fluxes in river beds. He defines it

as thermal skin effects and focuses on correcting the time lag that it generates. Therefore, for interpreting heating curves obtained at the heated cable it is necessary to acknowledge this effect.

The methods employing heated lines to quantify groundwater flux, imply the estimation of the aquifer thermal properties (Bakker et al., 2015; Hausner et al., 2016; Klepikova et al., 2011; Selker & Selker, 2018), especially thermal conductivity. Some authors integrate the estimation of the thermal conductivity within the method they use to interpret the temperature curves generated by the heating element (Bakker et al., 2015; Hausner & Kobs, 2016; Maldaner et al., 2018). Others rely on independent estimates (Gregory, 2009; Klepikova et al., 2011). Overall, this is a topic of intense research, not only because of its implications for obtaining accurate estimates of groundwater fluxes, but also because its relevance in the design of geothermal installations (Wang et al., 2010; Zhang et al., 2020), quantification of soil moisture (Ciocca et al., 2012) or seepage/recharge rates (Duque et al., 2016; Irvine et al., 2017). In fact, one of the most recent works by Zhang et al. (2020) provides an alternative to the use of TRT by using active fiber-optics, and discuss the topic at great length. Therefore, this paper will concentrate in discussing only the quantification of groundwater fluxes.

In order to overcome some of the aforementioned limitations of existing methods to quantify groundwater flux, we propose a new approach for the quantification of groundwater velocity and the thermal properties of the aquifer, which combines a new analytical method for the interpretation of the heating curves and a new approach for the cable installation. In contrast to other methodologies, we propose installing the FO cable in the annular space between the well casing and the aquifer. The installation of the cable outside the well casing aims to: (1) benefits from being conducted at the same time as the borehole installation process, (2) keeping the cable as in close contact as possible to the aquifer materials, and (3) maintaining the borehole available for the installation of additional monitoring devises. For the interpretation of the heating curves resulting from the active FO-DTS we propose a new analytical method. The interpretation methodology puts special emphasis on the estimation of the cable thermal effects in the heating curves. This methodology allows the interpretation of the heating curves generated at a single heating and monitoring cable, which simplifies field installation in many circumstances apart from those tested in this case. The presented method has been tested under controlled velocity conditions in a real sandy aquifer.

2. Problem Statement and Solution

The problem is conceptualized in order to provide an analytical methodology for designing and interpreting heat dissipation tests performed with a single FO cable. We start with a simplified ideal set-up: A line heat source in a homogeneous medium with horizontal flux (Figure 1a). Second, we discuss and consider in the analytical solution the effect of the cable materials (Figure 1b) to account for storage and skin effects, much like in well hydraulics. Finally, the proposed set-up involves the installation of the FO cable in the annular space of the piezometer. So, we solve the problem considering the field setup in which we have two parallel cables (Figure 1c), the one going down to the piezometer bottom and the same cable coming up to the surface with an unknown orientation with respect to the groundwater flow (Figure 1d).

2.1. Analytical Solution for the Ideal Case

The problem can be idealized as the temperature rise created by a small diameter heated cable embedded in a porous media where groundwater is flowing, which is governed by:

$$C_b \frac{\partial T}{\partial t} = \nabla \cdot \left(\left(\lambda \mathbf{I} + C_w \mathbf{D}_p \right) \cdot \nabla T \right) - C_w \mathbf{q} \cdot \nabla T + P\delta\left(\mathbf{x}\right) \tag{1}$$

where T [K] is the temperature, C_b [J/m^{3}K] is the bulk heat capacity, the term $\lambda \mathbf{I} + C_w \mathbf{D}_p$ is the thermal dispersion tensor $\mathbf{D}_T$[m^2/T], where λ [J/mK] is the thermal conductivity, $\mathbf{I}$ the identity tensor, C_w [J/m^{3}K] is the water heat capacity, $\mathbf{D}_p$ [m^2/s] the dispersion tensor, $\mathbf{q}$ [m/s] is the specific discharge and P [W/m] is the power released per unit length of cable. We take the x-axis along the flux direction perpendicularly to

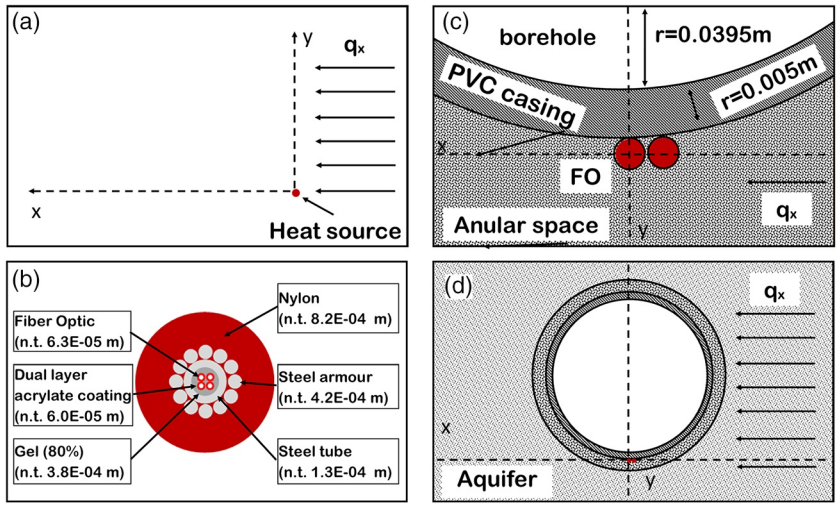

Figure 1. Description of the problem: (a) Idealized setting (Infinite Moving Line Source), (b) detailed cross-section of fiber-optic cable (n.t. = nominal thickness) (source: personal communication Brugg Kabel AG, Switzerland), (c) schematic cross-section of fiber-optic cable installation in the annular space, and (d) zoom out schematic horizontal cross-section of the field installation with indication of groundwater flux.

the cable. Therefore, $\mathbf{q} = \left(q_x, 0\right)$ and $\mathbf{D}_T$ is a diagonal tensor with principal components $D_{TL} = \lambda + C_w \alpha_{TL} q_x$, $D_{TT} = \lambda + C_w \alpha_{TT} q_x$, where α_{TL} and α_{TT} are, respectively, the longitudinal and transverse thermal dispersivities, much smaller than their solute transport counterparts. The solution to this problem for the purely conductive problem was presented by Carslaw & Jaeger (Carslaw & Jaeger, 1959; Stauffer et al., 2014).

The full solution for the dispersive problem is derived in the Appendix A. Actually, accounting for dispersion is somewhat controversial. Dispersion is often neglected (see discussion by Stauffer et al., 2014). Here, following the findings of Hidalgo et al. (2009): we use dispersion only to obtain the spatial distribution of temperature downstream, but neglect it to obtain temperature build-up at the source. That is, near the source, $\mathbf{D}_T = \lambda \mathbf{I}$, which allows simplifying the solution (Equation A-4) to

$$T\left(x, y, t\right) = \frac{P}{4\pi\lambda} e^{\frac{q_x C_w x}{2\lambda}} W_H\left(u, v\right); \text{with } u = \frac{C_b r^2}{4\lambda t}; \text{and } v = \frac{q_x C_w r}{2\lambda} \tag{2}$$

where r is the distance from the heating source, and W_H is the Hantush Well function (Hantush & Jacob, 1955) (Eq. A.7).

We have evaluated W_H using the approximation of Srivastava & Guzman-Guzman (1998), who also discuss the asymptotic behavior of W_H for small u (i.e., long time, advection dominated heat transport) and v (i.e., small q_x or r, conduction dominated transport). These two asymptotic behaviors, which can be observed in Figure 2a, are of interest. For small times and distances, advection can be neglected, and Equation 2 can be approximated as Theis (1935) well function, evaluated at the radius of the heated cable. Note that $t_0 \approx C_b \,/\, \lambda r_c^2$ is the time it takes for heat generated at $r = 0$ to reach r_c. In reality, the opposite might be a closer approximation (heat is generated on the armor and the sensor is in the center) (Figure 2b). We will return to this issue in Section 2.3. Theis solution is usually approximated as (Cooper & Jacob, 1946)

$$\mathrm{T}\left(\mathrm{r}, \mathrm{t}\right) = \frac{\mathrm{P}}{4\pi\lambda} \ln\left(\frac{2.25\lambda \mathrm{t}}{\mathrm{C_b r^2}}\right) \tag{3}$$

Equation 3 plots as a straight line versus log-time. The slope of this line m (K/log10 cycle) and the intercept with the log-t axis, t_0, can be used to derive λ and $\mathrm{C_b}$ as (Cooper & Jacob, 1946)

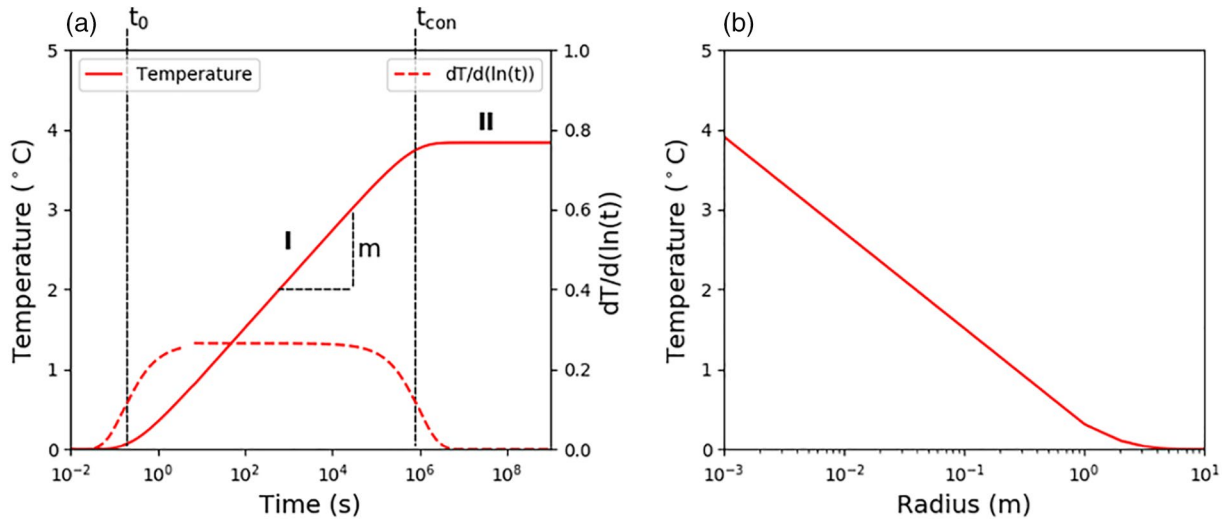

Figure 2. Behavior of analytical solution for an ideal case: (a) semi-log plot of temperature increase and its log-derivative (Equation 2). I and II indicate the conduction- and advection-dominated phases respectively. (b) Spatial distribution of temperature once steady state is reached (data: $\lambda_b = 3\ \mathrm{Wm^{-1}K^{-1}}$; $C_w = 4.2 \times 10^6\ \mathrm{Jm^{-3}K^{-1}}$; $C_b = 2.2 \times 10^6\ \mathrm{Jm^{-3}K^{-1}}$; $r = 0.001$ m, $P = 10\ \mathrm{Wm^{-1}}$; $q_x = 1.1 \times 10^{-6}\ \mathrm{m\ s^{-1}}$).

$$\lambda = \frac{\ln 10 \cdot \mathrm{P}}{4\pi m} = 0.183\frac{\mathrm{P}}{m} \tag{4a}$$

$$C_b = \frac{2.25\lambda t_0}{r^2} \tag{4b}$$

The distance affected by the temperature propagation due to conduction (R_{inf}) is:

$$R_{\mathrm{inf}} = \sqrt{\frac{2.5\lambda \mathrm{t}}{C_b}} \tag{5}$$

Heat within this radius of influence is dragged by the groundwater flux. In fact, Equation 2 can be viewed as an expression of the competition between conduction, which tends to increase temperature and R_{inf}, and advection, which drags heat away. Eventually, advection dominates heat transport (i.e., R_{inf} grows large enough for all the heat at the source to be dragged away), so that R_{inf} does not grow anymore and steady state is reached (i.e., temperature is stabilized). This is represented in Figure 2a by the "Advection-dominated" phase, which can be easily identified when the log-derivative tends to zero. Under these circumstances, the well function can be approximated as the Bessel function of second kind and order zero (K_0). Considering $x = 0$, the Equation 2 can be approximated as:

$$T_{(r,t=\infty)} = \frac{\boldsymbol{P}}{2\pi\lambda}\mathrm{K}_0\left(\frac{C_w q_x}{2\lambda}r\right) \tag{6}$$

Equation 6 represents the maximum temperature reached during heating, which depends on the specific discharge.

In summary, Equation 2 evaluated at the radius of the heating cable, behaves as Theis well function at early times, which can be approximated as a straight line after in semi-log plot (Equation 3) and tends to stabilize to a constant value, given by Equation 6, at late times. This behavior is illustrated in Figure 3 for several values of specific flux and typical values of thermal conductivity and heat capacity. In Figure 3a, the larger the groundwater flux the lower maximum temperature reached by the heating curve and the shorter the time it takes to reach this value. Figure 3b shows the maximum temperature as a function groundwater

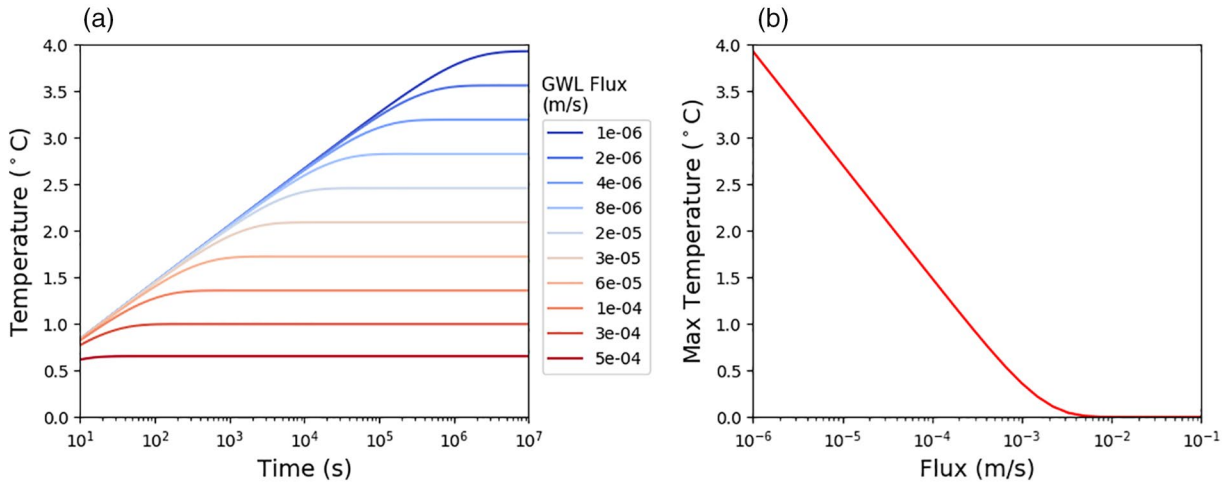

Figure 3. Sensitivity of the analytical solution to groundwater velocity: (a) Temperature evolution in time under different specific discharge rates. (b) Maximum temperature reach for a wide range of fluxes (data: $\lambda_b = 3\ \mathrm{Wm^{-1}K^{-1}}$; $C_w = 4.2 \times 10^6\ \mathrm{Jm^{-3}K^{-1}}$; $C_b = 2.2 \times 10^6\ \mathrm{Jm^{-3}K^{-1}}$; $r = 0.001$, $P = 10\ \mathrm{Wm^{-1}}$).

fluxes, giving an indication of the application range of the method for a given set of thermal properties of the media, power injection and cable radius.

We term conduction characteristic time (t_{con}) to the time when the conduction dominated and advection dominated behaviors intersect. It results from combining Equations 3 and 6, and it is given by:

$$t_{\mathrm{con}} = \frac{2.24\lambda C_b}{C_w^2 q_x^2} \tag{7}$$

Knowing t_{con} and λ, Equation 7 can be used to estimate groundwater velocity (q_x).

2.2. "Skin Effect" Correction

The simple conceptual model explained above (Figure 1a) do not consider the thermal effects induced by the cable materials through which heat has to travel before reaching the aquifer (Figure 1b). In reality, the obtained experimental heating curve is the combination of conduction heating transport within the cable, and an advection-conduction transport in the porous media once the heat reaches the cable walls.

In this study, we define the "skin effect" (ΔT_{sk}) as the temperature increase due to low thermal conductivity between the source of energy and the geological media surrounding the cable. This effect includes the low thermal conductivity of the isolation materials around the heating source. It also comprises any thermal interference of the installation around the cable (i.e., borehole), that may reduce the final maximum temperature reached at the aquifer materials (see Figure 1c). The skin effect can be expressed as an excess of temperature:

$$T_m = T\left(0, r, t\right) + \Delta T_{sk} \tag{8}$$

where T_m is the temperature at the measurement point, edge of the heating system, at a distance r from the center of the cable, where measures are taken. $T\left(0, \mathrm{r}, t\right)$ is the temperature calculated with Equation 2, thus the temperature without skin effect.

The skin effect due to the cable itself, depends on the thermal properties of the FO cable material. The glass fibers are protected with different layers for specific purposes. For the stainless steel armored multimode fiber-optic cable (Brugg Kabel AG, Switzerland) used in this study, the glass fibers are first covered with a

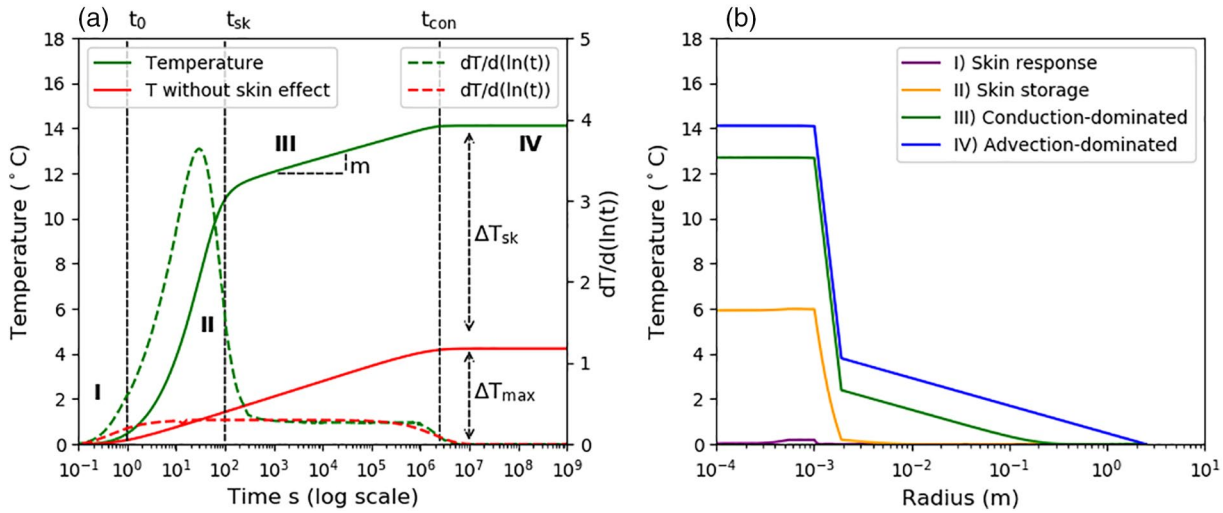

Figure 4. Behavior of temperature increase and its log-derivative when skin effect is present: (a) The heating curve with skin effect is compared with that resulting from applying the approximation from Srivastava & Guzman-Guzman (1998) to Equation 2. Evolution of temperature with skin effect considering all cable material from a heat transport model (data: $\lambda_w = 5.8 \times 10^{-1}$ Wm^{-1}K^{-1}; $\lambda_b = 3$ Wm^{-1}K^{-1}; $\lambda_{polyamide} = 9 \times 10^{-2}$ Wm^{-1}K^{-1}; $\lambda_{steel} = 16$ Wm^{-1}K^{-1}; $\lambda_{gel} = 0.3$ Wm^{-1}K^{-1}, $C_w = 4.2 \times 10^6$ Jm^{-3}K^{-1}; $C_b = 2.2 \times 10^6$ Jm^{-3}K^{-1}; $C_{polyamide} = 6.4 \times 10^6$ Jm^{-3}K^{-1}; $C_{steel} = 3.8 \times 10^6$ Jm^{-3}K^{-1}; $C_{gel} = 2.0 \times 10^6$ Jm^{-3}K^{-1}, $P = 10$ Wm^{-1}; $q_x = 1.1$e-6 m s^{-1}). The four heat transport regimes are indicated in the figure: (I) skin response, (II) skin dominated, (III) conduction dominated and (IV) advection dominated. (b) Spatial distribution of temperature at representative times for each heat transport regime.

dual layer acrylate coating, then embedded in a steel tube filled with a gel, then a steel armor and finally a nylon coating (Figure 1b). Due to its low thermal conductivity, the nylon coating is expected to produce the strongest contribution to the skin effect.

Exact estimation of the cable skin effect is not possible, since thermal properties of the cable materials are not provided by the manufacturer. However, if theoretical values and radius of each cable layer are considered in a heat transport model, the resulting heating curve would present an increase of temperature in the initial times which corresponds with the skin effect (Figure 4a). As a result, the initial conceptual model expands from two regimes to four regimes. (I) During the first seconds of heating, the materials surrounding the fiber delay in the response to the injected energy. This is the "skin response" regime. (II) The second regime presents a stable heating rate, representing the heat conduction through the cable materials. This phase may be named "skin dominated". (III) In a third stage, the cable is warm enough to transfer heat to the aquifer media. This sustained slope represents the heating rate, or "conduction-dominated" regime. (IV) Finally, the last stage occurs when temperature diffusion in the media reaches a limit due to advection, thus "advection-dominated" regime.

Ultimately, proper estimation of the groundwater velocity needs to be carried out once the skin effect is subtracted from the data. Skin effect can be roughly estimated graphically, with the difference between the heating curve and the curve without skin effect, thus the approximation for small times (Equation 3). Therefore, the analytical approach for the interpretation of the heating curves described in the previous section must be expanded with an additional step: (1) The slope of the conduction-dominated phase can be obtained graphically from the log derivative (dT/d (ln(t))), when this is constant but different from zero. The thermal conductivity of the porous media is then calculated with Equation 4a. (2) The skin effect can be subtracted knowing the initial time (t_0 in Figure 4a). This effective skin effect, results from the joined effect of the cable materials and any other material around the cable that might store heat. (3) From the initial time and using Equation 4b the bulk volumetric heat capacity can be estimated. (4) Finally, The conduction characteristic time (t_{con} in Figure 4a) can be graphically estimated from the intersection between the conduction-dominated and advection-dominated phases. Characteristic conduction time and previously estimated thermal conductivity are used to calculate the groundwater velocity from Equation 7.

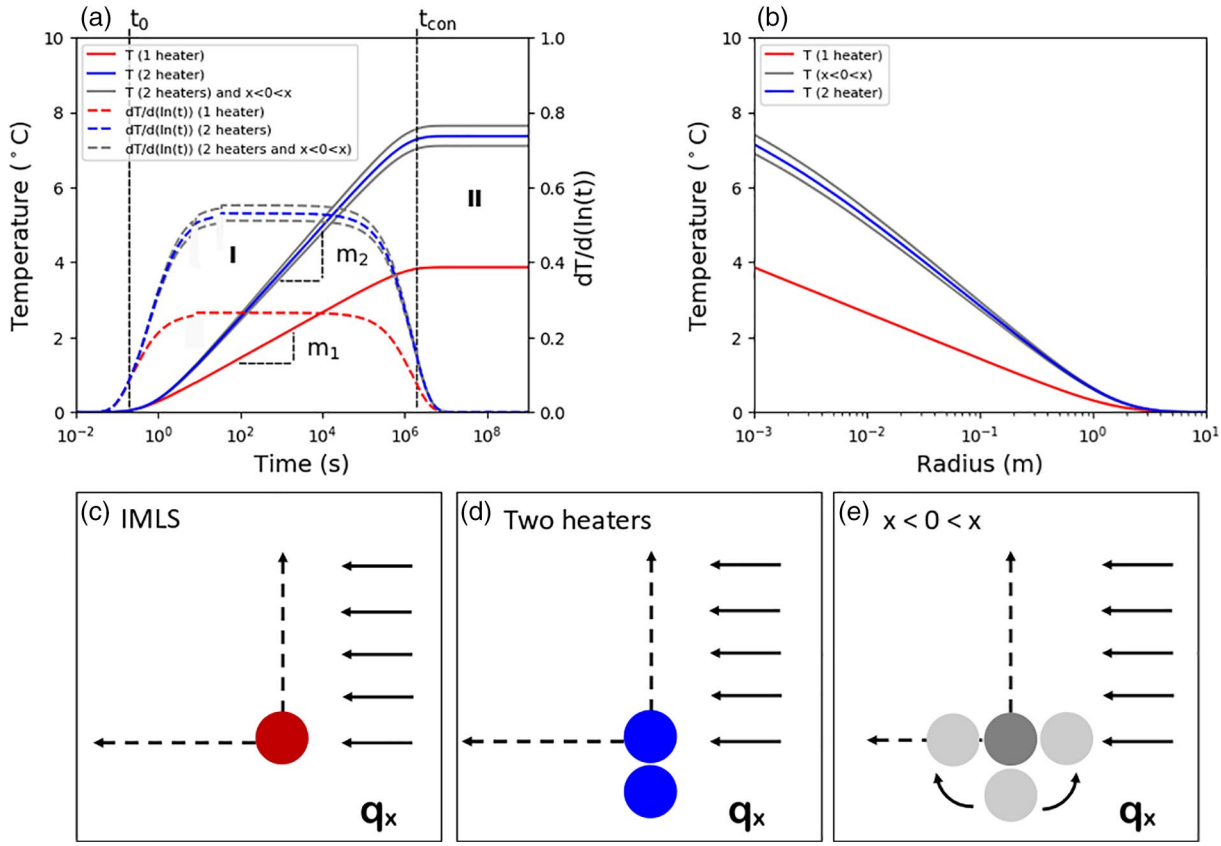

Figure 5. Conceptual model ranging from the ideal case to more complex scenarios where two cables are heated in parallel. (a) Comparison of the transient solution for the ideal case, thus with only one heater (red), for two heaters (blue), and for two heaters where the second could be in different position with respect to the direction of q_x and the observation point, thus x is different from zero (gray). "m_1" represents the slope of the ideal case, while "m_2" represents the slope of the case with two parallel heaters. (b) Stationary spatial distribution of temperature from the heater toward the aquifer matrix. (c) Graphical representation of the conceptual model for an Infinitesimal Moving Line Source (IMLS). (d) Graphical representation of the conceptual model for two parallel heat line sources. (e) Graphical representation of the conceptual model for two parallel heat line sources, where the position in x of the second heater is different from zero (data: $\lambda_b = 3\ \mathrm{Wm^{-1}K^{-1}}$; $C_w = 4.2 \times 10^6\ \mathrm{Jm^{-3}K^{-1}}$; $C_b = 2.2 \times 10^6\ \mathrm{Jm^{-3}K^{-1}}$; $P = 10\ \mathrm{Wm^{-1}}$; $r = 0.001$ m, $q_x = 1.1 \times 10^{-6}\ \mathrm{m\ s^{-1}}$).

2.3. Analytical Approach With Two Parallel Heaters

An additional deviation from the ideal case is the contribution of a second heater in parallel to the initial one to the temperature increment. This can be solved by superposition of the temperature increase due to each heating source, where a heater would be located in (x_1, y_1) and a second one in (x_2, y_2).

$$T_{(x,y,t)} = T_{1(x-x_1,y-y_1,t)} + T_{2(x-x_2,y-y_2,t)} \tag{9}$$

For the first heating source we consider r_1 equal to the radius of the heater. For the second heater, r_2 is the distance between the observation point (the center of the first heater) and the center of the second heater. Both heaters are considered to be located right next to each other (Figure 1c).

Figure 5 illustrates the difference between the analytical solution for an ideal case with one single heating source (Figure 5c), with the case of two parallel heating sources located at x_2 equal to zero (Figure 5d) and larger or smaller than zero (Figure 5e). In Figure 5a, it can be observed how temperature increment is doubled when a second heater is added close to the initial one. The effect of the position in x of the second heater is illustrated in Figure 5b by calculating the temperature for x_2 ranging between ±100 times r_2. In reality, this effect can be neglected if both cables are assumed to be right next to each other, thus x_2 ranging between ±2 times r_2.

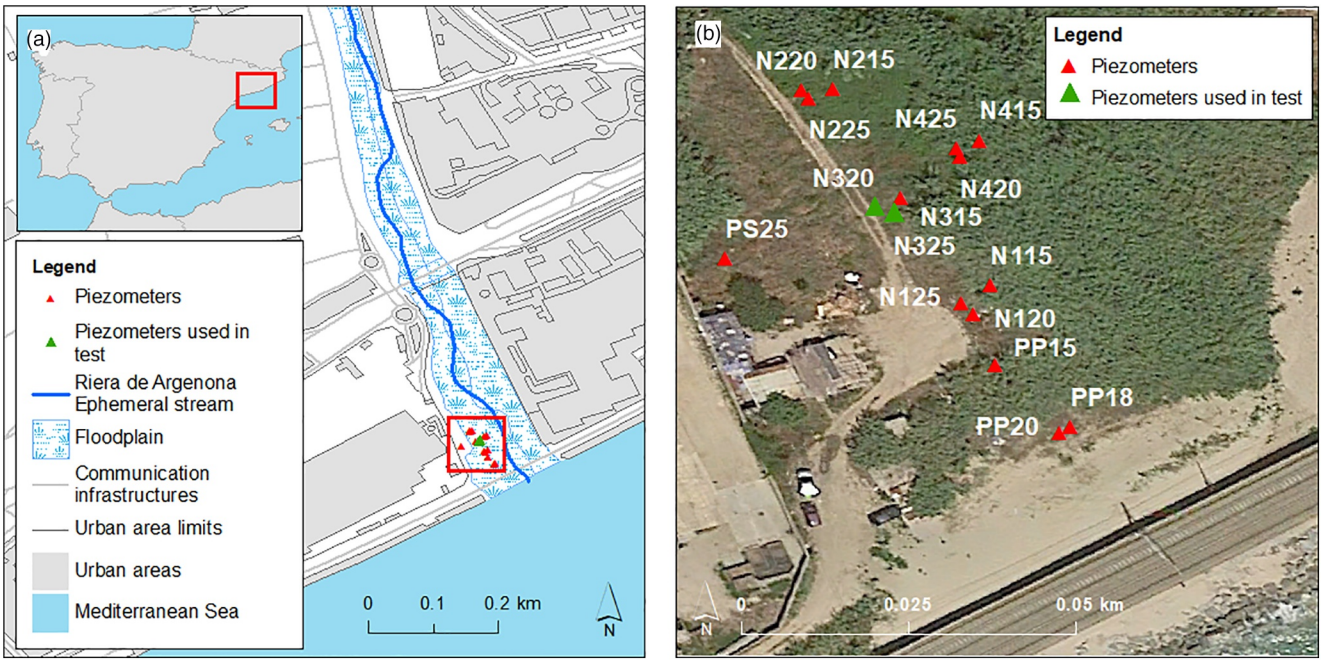

Figure 6. Location map: (a) Location experimental site; (b) distribution of piezometers in the field (sources: Institut Cartogràfic i Geològic de Catalunya [ICGC] and Agencia Catalana del Agua [ACA]).

Based on the mentioned conceptual model there are two parameters in our methodology that should be adapted to account for the contribution of a second heating cable, the input power and the distance between cables. As both cables are considered to be next to each other, the input power is considered to be doubled when estimating λ from Equation 4a. For the estimation of q_x, Equations 6 and 9 are combined to account for the temperature increase due to the second heater. In this case, r_1 and r_2 are the distances of each heater to the observation point (located in the center of the fiber-optic cable) respectively. Additionally, the effect of the second heater position (x_2) can be taken into consideration by not neglecting the exponential term in Equation 2 when approximating Equation 6. In this case, Equation 6 is resolved for $x_1 = 0$ and x_2 between 0 and r_2, where r_2 can be optimized within this range.

2.4. Application to a Real Case: Field Set-Up

The proposed approach for heat dissipation tests with FO-DTS at field scale was tested at the experimental site of MEDISTRAES (Folch et al., 2020). The experimental site is located in the alluvial aquifer of the Riera Argentona 40 km North from the city of Barcelona (Spain), between Catalan Littoral Mountain Range and Mediterranean Sea. Surface runoff only occurs during extreme rainfall events, therefore the "riera" or ephemeral stream runs dry most of the time. The catchment is dominated by granites and Palaeozoic materials covered by Quaternary alluvial sediments. The field site is therefore situated in the Quaternary deposits formed by a sequence of alternating horizontal layers of coarse (gravels and sands) to fine (silt and clay) deposits. The result is a strong vertical heterogeneity, which generates multiple aquifer levels separated by a few decimeter thick silt layers, whose confining effect is still under discussion. The bottom depth of these quaternary units is controlled by Paleozoic basement, having an average thickness close to the coast of 25–30 m (Agencia Catalana de L'Aigua, 2009).

The site comprises 16 shallow piezometers installed between 30 and 100 m from the seashore, with depths ranging between 15 and 25 meters (Figure 6). Most polyvinyl chloride (PVC) piezometers are screened only 2 m. Stainless steel armored multimode fiber-optic cable (Brugg Kabel AG, Switzerland) was installed along the annular space of the piezometers (Folch et al, under review). The cable was installed in a "*U*" shape, so that both cable extremes came out of the well (Figure 7). The cables were then connected in series in order to form two single fiber-optic lines that can be deployed individually. The connections were done with a

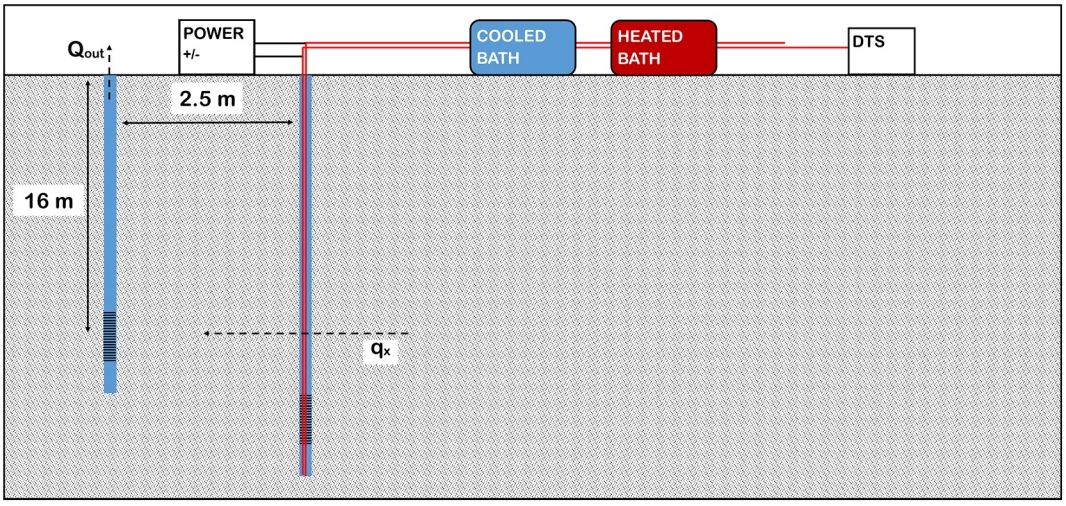

Figure 7. Schematic vertical cross-section of heat dissipation test field set-up. Deeper borehole represents the observation well (N325), and shallower borehole represented the pumping well (N320).

Prolite-40 Fusion Splicer (PROMAX, Spain) and an EFC-22 fiber-optic cutter (Ericson, Sweden). Each cable line has a length around 950 m with eight connections in each.

The cable was deployed with an Oryx + (Sensornet, UK) Distributed Temperature Sensor (DTS). The sensor has a minimum spatial sampling distance of 0.5 m and a minimum acquisition time of 10 s. For the purpose of this experiment, we chose a 10 s integration time, with a sampling frequency of 20 s, which then was increased to 30 s integration time and 2 min acquisition time after 4 h. FO lines were connected in a duplexed configuration (Hausner et al., 2011), and deployed in both directions, forward and reversed. Two calibration baths with different temperatures were installed at the beginning of the cable in order to invert the DTS raw signal into temperatures (Figure 7). Both baths are homogenized with small pumps (EHEIM Compact 300, EHEIM, Germany), and monitored with RBRsolo-T high resolution temperature loggers (RBR, Canada). The warm bath was constructed by submerging at least 10 m of cable in a 57-l portable coolers (Igloo, USA) filled of water, maintained at an average temperature of 38°C with a 150 W heater (Sera, Germany). The cold bath was constructed with additional 10 m of cable submerged in a 40-l thermoelectric portable cooler (MOBICOOL International Ltd., Hong Kong) filled with water kept at an average temperature of 10°C. DTS raw data are calibrated with the Single Ended Method (Hausner et al., 2011).

DTS raw data are transformed into temperature values using the Single Ended Calibration method. As proposed by Hausner et al. (2011), the quality of the calibration is reported through the root mean square error (RMSE) and duplexing error (E_{dup}). The first is calculated using the difference between calibrated and known temperatures at the calibration baths, representing the accuracy of the calibration. The second is calculated as the average of the difference between the duplexed calibrated temperatures, bringing information about the calibration consistency along the cable. During the first 4 h of the heat dissipation test, time integration period was set to 10 s. During this first period, the RMSE is 0.28°C and the E_{dup} is 0.08°C. After 4 h since heating started, the time integration period was set to 30 s, bringing the RMSE and the E_{dup} to 0.12°C and 0.09°C, respectively. For medium size cable lengths like this one, the selected time integration is the main limiting factor to temperature resolution. The initial seconds of the heat dissipation are crucial for the quantification of the skin effect. Therefore, the shortest integration period was chosen for the initial part of the heating dissipation test despite worsening of the temperature resolution.

3. Heat Dissipation Test

The Heat Dissipation Test implies heating a conducting element within the saturated soil until its temperature increase reaches steady state, while monitoring the temperature development of the heating element during heating and cooling phases. The FO cable used in this installation has a steel armor to provide

strength. This armor can be used to heat the cable due to the resistance to electric conduction that the metallic armor provides. A variable transformer (Carroll & Meynell, UK) was used to provide constant electric power of 1 W/m to the cable. The variable transformer was connected to either of the two sides of the FO cable sticking out of the well installation. Electricity injection was monitored with a multimeter. Although the variable transformer was set to 1 W/m, manual measurements with the multimeter gave 1.6 W/m, which is the value used to interpret the resulting data.

In order to test the method, the heat dissipation test was performed under known radial velocity conditions. Thus, while a constant-rate pumping test was being carried out in the installation, a suction pump was installed in piezometer N320 (Figure 6), pumping at a constant flow rate of 4 l/s during 2 days. Pumping rates were monitored with an electromagnetic velocity meter and kept constant during the test. During pumping and recovery, water levels were monitored in all piezometers using pressure sensors (LevelSCOUT 10 m, Seametrics, USA) programmed at a frequency of 2 min. The groundwater flux during steady state was estimated to be 5×10^{-5} m/s, by assuming uniform radial flux across a cylinder with height equal to the thickness of the unit between the two closest silt layers, and assuming they are fully confining (5 m) and radius equal the distance between the pumping well and the observation well (N325), which is 2.5 m (Figure 7).

Once the drawdown reached steady state, we started to heat the FO cable of the N325 piezometer. Heating at the N325 lasted for 1.5 days, enough to reach the steady-state of the heating curve at depths within the screened interval of the pumping well (N320).

4. Results

The test resulted in a set of heating curves vertically distributed along the observation well. Since the cable was installed in a "*U*" shape and the acquisition configuration ("duplexed") allowed for forward and reversed data, four heating curves are available per monitoring location. The distribution of maximum temperature reached at each depth (Figure 8a) gives an indication of the groundwater flux rate, where the lowest temperatures indicate the areas with the higher groundwater fluxes. In fact, the lowest maximum temperatures occur at the depths (14.8, 15.3, 15.8, and 16.3 m) confronting the screened interval of the pumping well (15–17 m). These are the only observation depths reaching steady state (Figure 8b), and thus, the only heating curves that can be interpreted with the proposed method.

Prior to any interpretation, the noise distorting the signal needs to be removed. In this case, a 2-fold objective will be addressed with the application of the Stable Computation of Log-derivatives from Ramos et al. (2017), to remove noise from temperature signal and compute the log-derivative.

The log-derivatives in combination with drawdown data are used for the identification of hydrogeological conceptual models responsible for the levels response to the hydraulic test (Renard et al., 2009) which are an analogy of the heat dissipation test for heat transport. The resulting log-derivative and smoothed data represented in Figure 9 for one of the selected depths, reveals the four phases of heating conceptual model identified in the analytical solutions, including the skin effect. The method is based on the analysis of the two last heating phases controlled by the aquifer thermal properties and advection.

First, the thermal conductivity is estimated. The log-derivative highlights two conduction phases with constant temperature increase attributed to the conduction within the cable materials ("Phase II - Skin storage") and to the conduction in the aquifer matrix ("Phase III - Conduction-dominated"). The last is used to estimate (Equation 4a) the thermal conductivity of the media, which is $1.2 \pm 7 \times 10^{-12}$ W/mºC (Figure 9).

The existence of a conduction phase associated to the heat storage in the cable materials, adds an additional temperature increase to the final temperature, the skin effect. The skin effect correction depends on the slope of the conduction-dominated phase and the initial time. However, as t_0 (Equation 4) is not known, it has to be adjusted. In fact, actual starting time is also uncertain (it has to be defined with seconds of accuracy). Given the delayed response of the cable to the heating and the limitation to 10 s of the DTS sampling frequency, it is difficult to measure directly. Because of this, we adjusted the actual starting time by trial and error during the log-derivative smoothing phase. Still, the thermal capacity is sensitive to t_0 (recall Equation 4b). Given the uncertainty about t_0, we decided to use a theoretical heat capacity of 2.71×10^6 J/m^3/K

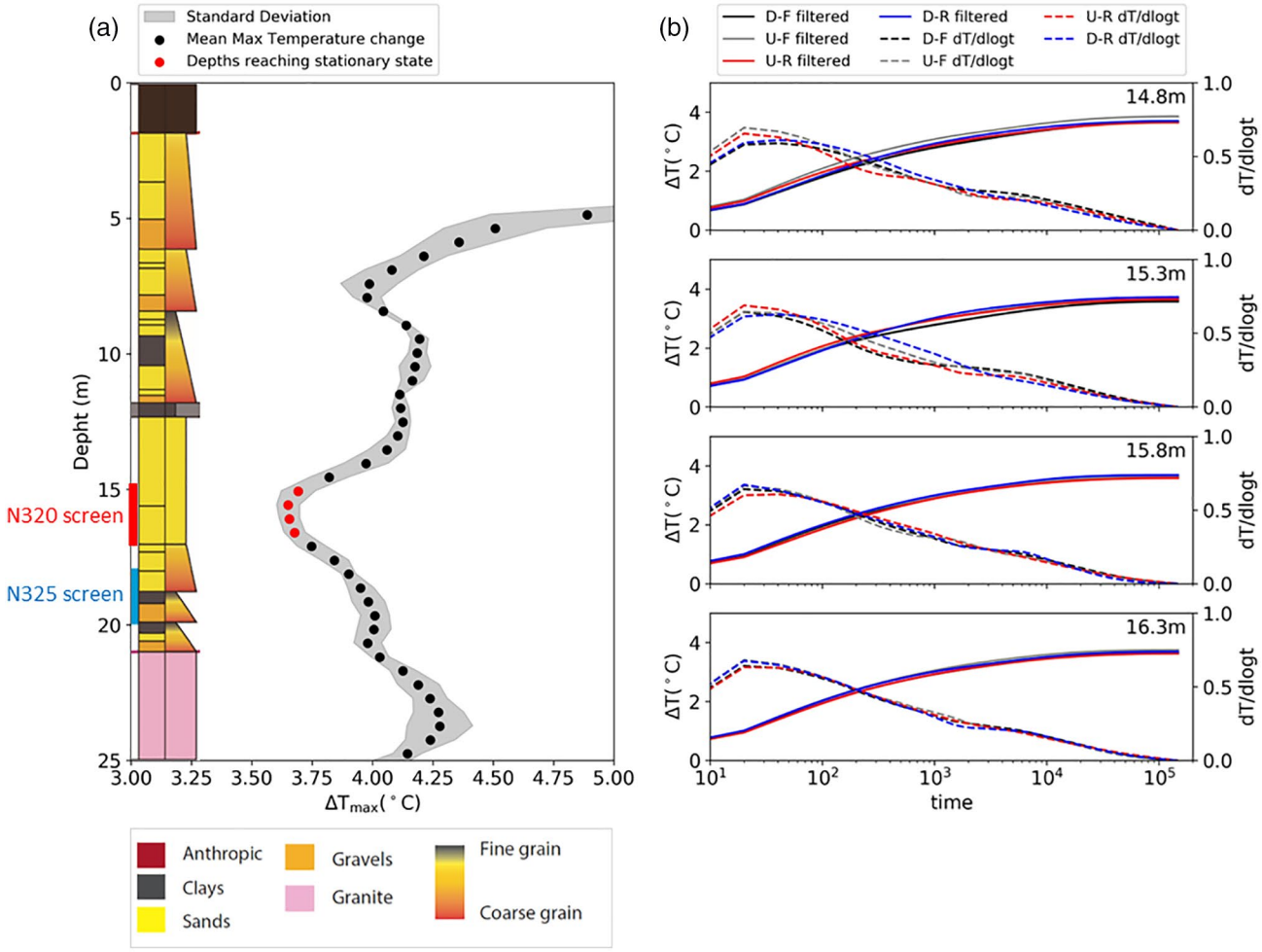

Figure 8. Results from the heat dissipation test: (a) Vertical distribution of average maximum temperatures reach during the Heat Dissipation Test. Mean values are calculated with the four available heating curves at the same depth (cable going up and down and the forward and reversed signals for each). Only heating curves at four specific depths reached steady state during the test. These are highlighted in red. (b) Evolution of temperature change and corresponding log derivative for each of the four depths reaching steady state. These smooth curves are the result of applying the filtering method of the Stable Computation of Log-derivatives to the original data. The nomenclature used in the legend represents the downwards (d) and upwards (U) sections of the cable, and the forward (f) and reversed (R) backscattered signals.

in the calculation of t_0 and the groundwater velocity. The resulting skin effect is estimated to be 1.54°C, thus a 33% (Equation 8) of the temperature increase is due to the cable materials.

Finally, groundwater velocity can be estimated by applying the analytical method in three different ways. The first approach uses the conduction characteristic time (t_{con}). This method does not require the skin effect correction, as it does not use the maximum temperature. Graphically, the t_{con} can be identified from the intersection between the aquifer conduction-dominated phase and the advection-dominated phase. The groundwater velocity was then estimated to be $4.3 \times 10^{-1} \pm 4 \times 10^{-17}$ m/s (Equation 7). In the second approach, we consider the effect of two parallel heaters through Equation 6. As there is no analytical solution to calculate q_x from this equation, q_x is obtained by interpolating the curve of $T_{(r,t=\infty)}$ versus q_x (Figure 3b). The estimated groundwater velocity was $2.3 \times 10^{-15} \pm 3 \times 10^{-16}$ m/s. The third approach considers both parallel heaters and their orientation with respect to the observation point and groundwater flow direction. A sensitivity analysis of Equation 9 was performed (data not shown), which resulted in the selection of an x value equal to the cable diameter. The estimated groundwater velocity using this last method was $2.8 \times 10^{-15} \pm 5 \times 10^{-16}$ m/s.

Figure 10 presents the vertical distribution and dispersion of the maximum temperatures (corrected for the skin effect), estimated thermal conductivities and groundwater fluxes for each depth that reaches

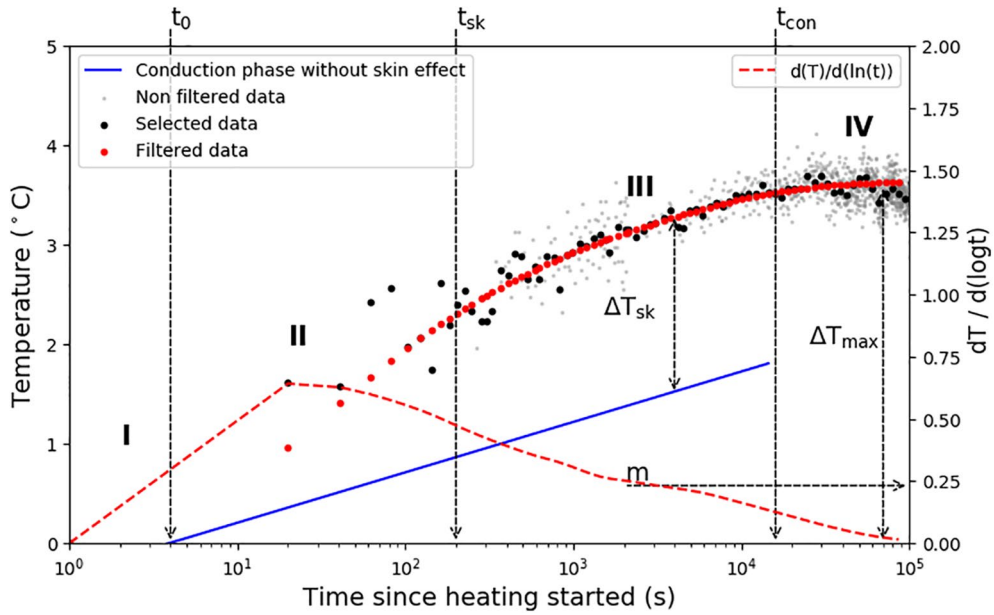

Figure 9. Heat dissipation curve at 15.8 m depth (black like in Figure 8a) in the observation well 2.5 m away from pumping well. Gray dots represent the raw temperature data after calibration of DTS signal. Black dots are the logarithmic selection of 100 points necessary to apply the filter. Red dots represent the signal after application of Stable Computation of Log-derivative filter. Red dashed line represents the computed Log-derivative. Blue line represents the aquifer conduction phase without skin effect used to approximate graphically the skin effect. Number represent the heat transport regimens: (I) skin response, (II) skin storage, (III) conduction dominated and (IV) advection dominated. These regimes are delimited by the characteristic times (t_0) initial time (t_{sk}) skin time and (t_{con}) conduction characteristic time. Estimation of the thermal conductivity is based on the conduction-dominated phase slope (m). DTS, Distributed Temperature Sensing.

steady-state. Groundwater flux estimates show larger variability when two heating lines are considered in the interpretation. Nevertheless, the analytical approaches considering two parallel heaters compare better to the groundwater flux estimates obtained from pumping rates than the estimates obtained by the method considering a single heating line.

5. Discussion

Measured heat dissipation curves (Figures 8 and 9) are similar to theoretical predictions (Figure 4). However, the actual estimated parameters are somewhat different to expected values. The estimated thermal conductivity (1.05–1.32 W/m°C, see Figure 10) is lower than theoretical values for a saturated sandy soil with a porosity of 0.35 (1.8–2.2 W/m°C; Stauffer et al., 2014). However, lithology indicates the presence of silty/clay layers, with a much lower thermal conductivity (0.9–2.3 W/m°C; Stauffer et al., 2014). Therefore, although the deposits where the screen interval of the pumping well (N320) are located in a predominantly sandy layer, a percentage (not known) of silt is expected to be present, lowering the thermal conductivity. Presence of organic matter, with low thermal conductivity of around 0.5 W/m°C (Mckenzie et al., 2007), in the sediments is also frequent in near shore areas (Duque et al., 2016). In fact, large spatial variations of thermal conductivity are common in near shore areas (Duque et al., 2016), where deposition of organic matter and fine sediments mix with larger grain deposits. Additionally to the matrix heterogenic composition, the presence of the PVC borehole casing, with a much lower thermal conductivity, near the FO cable may be an additional cause for the unexpected low thermal conductivity.

Estimated groundwater velocity in the same order of magnitude of the value obtained from the pumping rate (5×10^{-15} m/s). Still, the slightly smaller value of the estimated groundwater velocity could be related to different reasons belonging to three main groups: (1) water flow assumptions and (2) analytical approach and postprocessing of the FO-DTS data, and (3) the field set-up and Heat Dissipation Test implementation.

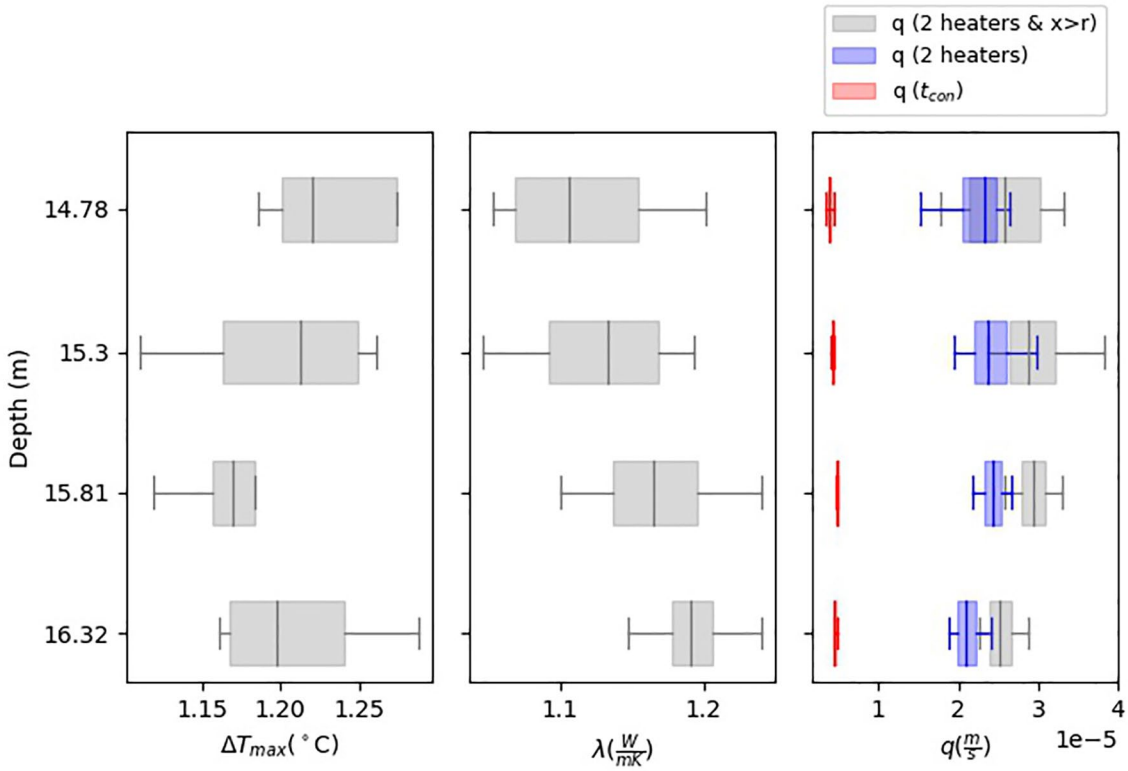

Figure 10. Boxplots illustrating the vertical distribution of maximum temperatures without skin effect, thermal conductivity and groundwater velocity. Box plots distribution is calculated for each depth where temperature reaches steady-state, with the four available heating curves (Figure 8b). The colors of the boxplots illustrate the variability of the three different analytical approaches to estimate q_x.

Regarding the first, groundwater flux was estimated under the assumption of homogeneous horizontal radial flow. This assumption sounds realistic because the aquifer presents strong vertical heterogeneities, which might concentrate velocity through localized layers. Moreover, piezometers are partially penetrating (only 2 m open interval) which leads to vertical fluxes toward the screened section. In fact, all piezometers responded to pumping (data not shown), which suggests that flow might be spherical toward the screened interval. Worse, the most conductive layer does not appear to be the one we tested, but the one below. In this case, one should expect a significant vertical flow near the well and a reduction of the radial component. In short, flux direction and magnitude can be modified in the vicinity of the observation piezometer, which might lead to an over or underestimation of the flux, with respect to assumed ideal radial flow. Therefore, the identified discrepancy between the groundwater velocity derived from the heating curves and thus derived from the pumping test, might come from the interpretation of the latter.

Discrepancies may also be caused by difficulties with the test itself. These difficulties may be of two kinds: (1) the analytical approach and postprocessing of the FO-DTS data, and (2) the field set-up and Heat Dissipation Test implementation. While the conceptual model accounts for cable and borehole thermal effects ("skin effect"), further research needs to be to characterize cable materials and proper quantification of the skin effect. Additionally, the application of the analytical approach requires graphical identification of the conduction-dominated phase slope (m), initial time (t_0), and conduction characteristic time (t_{con}) which has associated some deviation. For example, for the estimation of the thermal conductivity, the lack of a constant plateau in the temperature log-derivate from which to infer the slope of the conduction-dominated phase adds uncertainty to the method. Moreover, this slope may also be affected by a later skin effect generated by the PVC borehole casing. Uncertainty in the slope and in t_0, coupled to the low early time sampling frequency provided by the DTS, cause some uncertainty in the estimation of thermal conductivity and water flux. Finally, noise removal algorithms and graphical interpretation are a source of uncertainty, as they depend on the user knowledge about the conceptual model underlying the data.

Referring to the field application of the method, some sources of uncertainty can arise from the installation of the cable and performance of the heat dissipation test. The main difficulty of the cable installation was to reduce the amount of connections along the cable. Additionally, the method proved highly sensitive to a possible separation between both cables and the relative orientation of them with respect to the flux. Given the complexity of the installation, it is easy to imagine both cables might be separated several centimeters at certain points, resulting in a considerable error when solving Equation 9. When performing the heat dissipation test, ensuring cable constant heating requires periodic monitoring of intensity and voltage evolution in order to validate constant power injection. Additionally, selection of power to be injected depends on the electric installation and the cable length to be heated. The longer the cable the higher power the system will require in order to reach the same power per unit length of cable. Fortunately, in this case, power injection should be minimized to avoid convective fluxes, yet another limitation of the method. One of the major sources of uncertainty in the interpretation of the data is the maximum acquisition frequency of DTS, in this case 10 s. Exact monitoring of the heating initial time is essential for proper characterization of the heating curve, as the method is very sensitive to the initial time and skin effect values that depend on the initial moments of the heating curve.

6. Conclusion

We presented a new methodological approach to perform heat dissipation tests with a single FO cable in order to quantify groundwater fluxes and thermal properties. The method is based on the interpretation of the heat dissipation curves generated by a single heating and monitoring FO cable, situated between the piezometer and the aquifer matrix outside the well casing. Complementarily, a new approach to approximate the existing MILS analytical solution was presented for the interpretation of the heat dissipation curves. A correction for the skin effect generated by the low thermal conductivity of the cable and borehole materials is included in the interpretation. The proposed methodology to interpret the heating curves comprises five steps; (1) temperature calibration, (2) noise removal, computation of temperature log-derivative and conceptual model identification, (3) skin effect correction, (4) estimation of thermal properties from conduction-dominated phase slope and initial time, and (5) estimation of groundwater velocity with conduction characteristic time or corrected maximum temperature.

There are three main contributions of this study: (1) the field set-up to carry out heat dissipation tests, (2) the approach to approximate and adapt the existing analytical solution to the interpretation of the resulting heating curves, including the consideration of the cable "skin effect", and (3) the testing of both at the field scale. Furthermore, the proposed method has several advantages: (i) FO-DTS is installed as an additional downhole technology, which can be deployed in parallel to other borehole devices, (ii) the single heating-monitoring cable approach reduces costs and simplifies its installation, and (iii) the analytical approach provides a simple way to interpret heating curves, likewise well hydraulic analytical solutions.

The method presented is a step toward generalized use of heat dissipation tests with FO-DTS not only for aquifer hydraulic characterization but also for the hydrology field. Obtained results are consistent with the expected values of groundwater flux. Still, we attribute the small discrepancy present in the results to the effect of different uncertainties (soil heterogeneity, vertical fluxes or thermal properties of cable and borehole materials). The identified uncertainties and problems are thoroughly discussed, providing valuable practical information for the improvement and replication of the test. In this line, further research is needed to overcome part of these uncertainties both at the field and during interpretation of the data. Improving quantification of the "skin" and aquifer heterogeneity effects are identified as priority topics for future research.

Appendix A

The solution of Equation 1 for a unit heat pulse input is

$$T_1\left(x,y,t\right)=\frac{1}{2\pi C_b\sigma_x\sigma_y}\exp\left[-\frac{1}{2}\left(\left(\frac{x-v_Tt}{\sigma_x}\right)^2+\left(\frac{y}{\sigma_y}\right)^2\right)\right] \tag{A.1}$$

where $\sigma_x=\sqrt{2D_{TL}t/C_b}$, $\sigma_y=\sqrt{2D_{TT}t/C_b}$, and $v_T=q_xC_w/C_b$. This equation can be somewhat simplified by defining $t_{cD}=C_b\left(x^2/D_{TL}+y^2/D_{TT}\right)$ and $x_c=2D_{TL}/C_bv_T$

$$T_1\left(x,y,t\right)=\frac{1}{4\pi\sqrt{D_{TL}D_{TT}}\,t}e^{x/x_c}\exp\left[-\frac{1}{4}\left(\frac{t_{cD}}{t}+\frac{C_bv_T^2t}{D_{TL}}\right)\right] \tag{A.2}$$

The solution for a continuous energy source P can be obtained by convolution, which yields

$$T=\frac{P}{4\pi\sqrt{D_{TL}D_{TT}}}e^{x/x_c}\int_0^t\frac{1}{\tau}\exp\left[-\frac{1}{4}\left(\frac{t_{cD}}{\tau}+\frac{2v_T\tau}{x_c}\right)\right]d\tau \tag{A.3}$$

We transform variables by choosing $s=t_{cD}/4\tau$, so that $d\tau/\tau=-ds/s$. With this transformation, Equation (3.14) becomes:

$$T=-\frac{P}{4\pi\sqrt{D_{TL}D_{TT}}}e^{x/x_c}\int_\infty^{t_{cD}/4t}\frac{1}{s}\exp\left[-s-\frac{v_Tt_{cD}}{8x_cs}\right]ds \tag{A.4}$$

Exchanging the integral limits, we get:

$$T=\frac{P}{4\pi\sqrt{D_{TL}D_{TT}}}e^{x/x_c}W_H\left(\frac{t_{cD}}{4t},\sqrt{\frac{v_Tt_{cD}}{2x_c}}\right) \tag{A.5}$$

Where W_H is known in well hydraulics literature Hantush (1955) well function, defined as:

$$W_H\left(a,b\right)=\int_a^\infty\frac{1}{s}\exp\left[-s-\frac{b^2}{4s}\right]ds \tag{A.6}$$

The log-derivative of T is

$$\frac{dT}{dlnt}=\frac{P}{\pi\sqrt{D_{TL}D_{TT}}}e^{x/x_c}\frac{t}{t_{cD}}\exp\left[-\frac{t_{cD}}{4t}-\frac{v_Tt}{2x_c}\right] \tag{A.7}$$

Or, assuming dispersivities to be zero

$$T_D\left(x_D,y_D,t_D\right)=\frac{P}{4\pi\lambda}e^{\left(\frac{C_wq_x}{2\lambda}x\right)}W_H\left(\frac{C_br^2}{4\lambda t},\frac{C_wq_x}{2\lambda}r\right) \tag{A8}$$

Acknowledgments
This work was funded by the projects CGL2016-77122-C2−1−R / 2-R and PID2019-110212RB-C22 / C21 of the Spanish Government. We would like to thank SIMMAR (Serveis Integrals de Manteniment del Maresme) and the Consell Comarcal del Maresme in the construction of the research site. We would like to acknowledge Sensornet (UK) for their support and collaboration. We would also like to thank Dr. Javier Benitez Buelga for his collaboration in designing and setting up the fiber-optic field installation. The author Albert Folch is a Serra Húnter Fellow.

Data Availability Statement

The paper provides all the information needed to replicate the results. All experimental data related to the analysis performed can be downloaded from https://doi.org/10.5281/zenodo.3820500.

References

Agencia Catalana de L'Aigua (2009). Maresme 18. Fitxa de Caracterització, análisis de pressions, impactes i análisis del risc d'incompliment. In *Fitxes de Caracterització inicial, pressions i Impactes de les Masses d'Aigua Subterrànies (IMPRESS, 2004)*, Barcelona. Retrieved from http://aca536web.gencat.cat/aca/appmanager/aca/aca?_nfpb=true&_pageLabel=P2540018196537126804673621 8&_nfls=false

Anderson, M. P. (2005). Heat as a ground water tracer. *Ground Water*, *43*(6), 951–968. https://doi.org/10.1111/j.1745-6584.2005.00052.x

Bakker, M., Calj, R., Schaars, F., Made, K.-J., & Haas, S. (2015). An active heat tracer experiment to determine groundwater velocities using fiber optic cables installed with direct push equipment. *Water Resources Research*, *51*, 2760–2772. https://doi.org/10.1002/2014WR016632.Received

Bandos, T. V., Montero, Á. E., Fernández de Córdoba, P. J., & Urchueguía, J. F. (2011). Improving parameter estimates obtained from thermal response tests: Effect of ambient air temperature variations. *Geothermics*, *40*(2), 136–143. https://doi.org/10.1016/j.geothermics.2011.02.003

Banks, E. W., Shanafield, M. A., & Cook, P. G. (2014). Induced temperature gradients to examine groundwater flowpaths in open boreholes. *Ground Water*, *52*(6), 943–951. https://doi.org/10.1111/gwat.12157

Bense, V. F., Read, T., Bour, O., Le Borgne, T., Coleman, T., Krause, S., et al. (2016). Distributed Temperature Sensing as a downhole tool in hydrogeology. *Water Resources Research*, *52*(12), 9259–9273. https://doi.org/10.1002/2016WR018869

Cardenas, M. B. (2010). Thermal skin effect of pipes in streambeds and its implications on groundwater flux estimation using diurnal temperature signals. *Water Resources Research*, *46*, W03536. https://doi.org/10.1029/2009WR008528

Carslaw, H. S., & Jaeger, J. C. (1959). *Conduction of heat in soils* (2nd ed.). Great Britain:Oxford University Press.

Ciocca, F., Lunati, I., Van de Giesen, N., & Parlange, M. B. (2012). Heated optical fiber for distributed soil-moisture measurements: A Lysimeter Experiment. *Vadose Zone Journal*, *11*(4), vzj2011.0199. https://doi.org/10.2136/vzj2011.0199

Coleman, T. I., Parker, B. L., Maldaner, C. H., & Mondanos, M. J. (2015). Groundwater flow characterization in a fractured bedrock aquifer using active DTS tests in sealed boreholes. *Journal of Hydrology*, *528*, 449–462. https://doi.org/10.1016/j.jhydrol.2015.06.061

Cooper, H. H., & Jacob, C. E. (1946). A generalized graphical method for evaluating formation constants and summarizing well-field history. *Eos, Transactions American Geophysical Union*, *27*(4), 526–534. https://doi.org/10.1029/TR027i004p00526

Davis, S. N., Campbell, D. J., Bentley, H. W., & Flynn, T. J. (1985). *Ground-water traces*. Worthington, OH: National Water Well Association.

des Tombe, B. F., Bakker, M., Smits, F., Schaars, F., & van der Made, K. J. (2019). Estimation of the variation in specific discharge over large depth using Distributed Temperature Sensing (DTS) measurements of the heat pulse response. *Water Resources Research*, *55*(1), 811–826. https://doi.org/10.1029/2018WR024171

Drost, W., Klotz, D., Koch, A., Moser, H., Neumaier, F., & Rauert, W. (1968). Point dilution methods of investigating ground water flow by means of radioisotopes. *Water Resources Research*, *4*(1), 125–146. https://doi.org/10.1029/WR004i001p00125

Duque, C., Müller, S., Sebok, E., Haider, K., & Engesgaard, P. (2016). Estimating groundwater discharge to surface waters using heat as a tracer in low flux environments: The role of thermal conductivity. *Hydrological Processes*, *30*(3), 383–395. https://doi.org/10.1002/hyp.10568

Feng, Q., & Zhan, H. (2016). Integrated aquitard-aquifer flow with a mixed-type well-face boundary and skin effect. *Advances in Water Resources*, *89*, 42–52. https://doi.org/10.1016/j.advwatres.2016.01.003

Folch, A., Val, L., Luquot, L., Martínez-Pérez, L., Bellmunt, F., Lay, H. L., et al. (2020). Combining Fiber Optic (FO-DTS), Cros Hole ERT and time lapse formation electrical conductivity to characterize and monitor a coastal aquifer. *Journal of Hydrology*, *588*, 125050. https://doi.org/10.1016/j.jhydrol.2020.125050

Freifeld, B. M., Daley, T. M., Hovorka, S. D., & Henninges, J. (2008). Recent advances in well-based monitoring of CO_2 sequestration. *Energy Procedia*, *1*, 2277–2284

Giese, R., Henninges, J., Lüth, S., Morozova, D., & Schmidt-hattenberger, C. (2009). Energy Procedia Monitoring at the CO2SINK Site : A concept integrating geophysics, geochemistry and microbiology. *Energy Procedia*, *1*(1), 2251–2259. https://doi.org/10.1016/j.egypro.2009.01.293

Gregory, C. T. (2009). *Temperature and infiltration characterization of a constructed wetland for waste water treatment*. Oregon State University. Retrieved from http://ir.library.oregonstate.edu/concern/graduate_thesis_or_dissertations/5999n5628

Hantush, M. S., & Jacob, C. E. (1955). Non-steady radial flow in an infinite leaky aquifer. *Eos, Transactions American Geophysical Union*, *36*(1), 95–100. https://doi.org/10.1029/TR036i001p00095

Hausner, M. B., & Kobs, S. (2016). Identifying and correcting step losses in single-ended fiber-optic distributed temperature sensing data. *Journal of Sensors*, *2016*, 1–10. https://doi.org/10.1155/2016/7073619

Hausner, M. B., Kryder, L., Klenke, J., Reinke, R., & Tyler, S. W. (2016). Interpreting variations in groundwater flows from repeated distributed thermal perturbation tests. *Ground Water*, *54*(4), 559–568. https://doi.org/10.1111/gwat.12393

Hausner, M. B., Suárez, F., Glander, K. E., van de Giesen, N., Selker, J. S., & Tyler, S. W. (2011). Calibrating single-ended fiber-optic Raman spectra distributed temperature sensing data. *Sensors*, *11*(11), 10859–10879. https://doi.org/10.3390/s111110859

Hidalgo, J. J., Carrera, J., & Dentz, M. (2009). Steady state heat transport in 3D heterogeneous porous media. *Advances in Water Resources*, *32*(8), 1206–1212. https://doi.org/10.1016/j.advwatres.2009.04.003

Irvine, D. J., Kurylyk, B. L., Cartwright, I., Bonham, M., Post, V. E. A., Banks, E. W., et al. (2017). Groundwater flow estimation using temperature-depth profiles in a complex environment and a changing climate. *Science of the Total Environment*, *574*, 272–281. https://doi.org/10.1016/j.scitotenv.2016.08.212

Jamin, P., Goderniaux, P., Bour, O., Le Borgne, T., Englert, A., Longuevergne, L., et al. (2015). Contribution of the finite volume point dilution method for measurement of groundwater fluxes in a fractured aquifer. *Journal of Contaminant Hydrology*, *182*, 244–255. https://doi.org/10.1016/j.jconhyd.2015.09.002

Klepikova, M. V., Le Borgne, T., Bour, O., & Davy, P. (2011). A methodology for using borehole temperature-depth profiles under ambient, single and cross-borehole pumping conditions to estimate fracture hydraulic properties. *Journal of Hydrology*, *407*(1–4), 145–152. https://doi.org/10.1016/j.jhydrol.2011.07.018

Leaf, A. T., Hart, D. J., & Bahr, J. M. (2012). Active thermal tracer tests for improved hydrostratigraphic characterization. *Ground Water*, *50*(5), 726–735. https://doi.org/10.1111/j.1745-6584.2012.00913.x

Liu, G., Knobbe, S., & Butler, J. J. (2013). Resolving centimeter-scale flows in aquifers and their hydrostratigraphic controls. *Geophysical Research Letters*, *40*(6), 1098–1103. https://doi.org/10.1002/grl.50282

Maldaner, C. H., Munn, J. D., Coleman, T. I., John, W., & Parker, B. L. (2018). Groundwater flow quantification in fractured rock boreholes using active distributed temperature sensing under natural gradient conditions. *Water Resources Research*, *55*, 3285–3306. https://doi.org/10.1029/2018WR024319

Mckenzie, J. M., Siegel, D. I., Rosenberry, D. O., Glaser, P. H., & Voss, C. I. (2007). Heat transport in the Red Lake Bog. *Glacial Lake Agassiz Peatlands*, *378*, 369–378. https://doi.org/10.1002/hyp

Perzlmaier, S., Auñeger, M., & Conrad, M. (2004). Distributed fiber optic temperature measurements in hydraulic engineering: Prospects of the heat-up method. *Proceedings of the 72nd ICOLD Annual Meeting Workshop on Dam Safety Problems and Solutions-Sharing Experience*, 1–16.

Pitrak, M., Mares, S., & Kobr, M. (2007). A simple borehole dilution technique in measuring horizontal ground water flow. *Ground Water*, *45*(1), 89–92. https://doi.org/10.1111/j.1745-6584.2006.00258.x

Ramos, G., Carrera, J., Gómez, S., Minutti, C., & Camacho, R. (2017). A stable computation of log-derivatives from noisy drawdown data. *Water Resources Research*, *53*(9), 7904–7916. https://doi.org/10.1002/2017WR020811

Raymond, J., Therrien, R., Gosselin, L., & Lefebvre, R. (2011). Numerical analysis of thermal response tests with a groundwater flow and heat transfer model. *Renewable Energy*, *36*(1), 315–324. https://doi.org/10.1016/j.renene.2010.06.044

Read, T., Bour, O., Bense, V., Le Borgne, T., Goderniaux, P., Klepikova, M. V., et al. (2013). Characterizing groundwater flow and heat transport in fractured rock using fiber-optic distributed temperature sensing. *Geophysical Research Letters*, *40*(10), 2055–2059. https://doi.org/10.1002/grl.50397

Read, T., Bour, O., Selker, J. S., Bense, V. F., Le Borgne, T., Hochreutener, R., et al. (2014). Active-distributed temperature sensing to continuously quantify vertical flow in boreholes. *Water Resources Research*, *50*(5), 3706–3713. https://doi.org/10.1002/2014WR015273

Reiter, M. (2001). Using precision temperature logs to estimate horizontal and vertical groundwater flow components. *Water Resources Research*, *37*(3), 663–674. https://doi.org/10.1029/2000WR900302

Renard, P., Glenz, D., & Mejias, M. (2009). Understanding diagnostic plots for well-test interpretation. *Hydrogeology Journal*, *17*(3), 589–600. https://doi.org/10.1007/s10040-008-0392-0

Sánchez-Vila, X., Axness, C. L., & Carrera, J. (1999). Upscaling transmissivity under radially convergent flow in heterogeneous media. *Water Resources Research*, *35*(3), 613–621. https://doi.org/10.1029/1998WR900056

Selker, F., & Selker, J. (2018). Investigating water movement within and near wells using active point heating and fiber optic distributed temperature sensing. *Sensors*, *18*(4), 1023. https://doi.org/10.3390/s18041023

Sellwood, S. M., Hart, D. J., & Bahr, J. M. (2015). Evaluating the use of in-well heat tracer tests to measure. *Borehole Flow Rates*, *35*(4), 85–94. https://doi.org/10.1111/gwmr.12134

Srivastava, R., & Guzman-Guzman, A. (1998). Practical approximations of the well function. *Ground Water*, *36*(5), 844–848.Retrieved from https://doi.org/10.1111/j.1745-6584.1998.tb02203.x

Stauffer, F., Bayer, P., Blum, P., Molina-Giraldo, N., & Kinzelbach, W. (2014). *Thermal Use of shallow groundwater (I)*. Taylor & Francis Group, LLC.

Su, H., Tian, S., Cui, S., Yang, M., Wen, Z., & Xie, W. (2016). Distributed optical fiber-based theoretical and empirical methods monitoring hydraulic engineering subjected to seepage velocity. *Optical Fiber Technology*, *31*, 111–125. https://doi.org/10.1016/j.yofte.2016.05.008

Taniguchi, M. (1993). Evaluation of vertical groundwater fluxes and thermal properties of aquifers based on transient temperature-depth profile. *Water Resources Research*, *29*(7), 2021–2026. https://doi.org/10.1029/93WR00541

Theis, C. V. (1935). The relation between the lowering of the Piezometric surface and the rate and duration of discharge of a well using groundwater storage. *Eos, Transactions American Geophysical Union*, *16*(2), 519–524. https://doi.org/10.1029/TR016i002p00519

Tsang, C. F., Hufschmied, P., & Hale, F. V. (1990). Determination of fracture inflow parameters with a borehole fluid conductivity logging method. *Water Resources Research*, *26*(4), 561–578. https://doi.org/10.1029/WR026i004p00561

Wagner, V., Blum, P., Kübert, M., & Bayer, P. (2013). Geothermics analytical approach to groundwater-influenced thermal response tests of grouted borehole heat exchangers. *Geothermics*, *46*, 22–31. https://doi.org/10.1016/j.geothermics.2012.10.005

Wang, H., Qi, C., Du, H., & Gu, J. (2010). Improved method and case study of thermal response test for borehole heat exchangers of ground source heat pump system. *Renewable Energy*, *35*(3), 727–733. https://doi.org/10.1016/j.renene.2009.08.013

Zhang, B., Gu, K., Shi, B., Liu, C., Bayer, P., Wei, G., et al. (2020). Actively heated fiber optics based thermal response test: A field demonstration. *Renewable and Sustainable Energy Reviews*, *134*, 110336. https://doi.org/https://doi.org/10.1016/j.rser.2020.110336